hinterland. Examples include the 3,074-Myr-old dacitic to rhyolitic upper Dominion group, and the felsic volcanics and agglomerates of the Kraaipan group, also tentatively dated at ~3,070 Myr (L.J.R., D.W.D., S.L.K. and C. R. Anhaeusser). The Gaborone granite in southeastern Botswana, recently dated at 2,790 Myr (D.W.D., L.J.R., D. F. Grobler and M. C. Jackson, manuscript in preparation), is now known to be genetically related to an extensive province of, now largely eroded, rhyolitic volcanics. This province, previously thought to be Proterozoic in age[17], formed during Central Rand group deposition. It may have been a locus for high-level gold mineralization, as minor silver-base metal veins have been reported from remnants of the rhyolites surrounding the Gaborone granite[18]. The erosion of high-level felsic plutonic-volcanic suites, mineralized by associated mesothermal to epithermal fluid systems would seem, in the light of our data, to offer a reasonable solution for the source of Witwatersrand gold.

The complex sequence of events involving uranium specificity, consecutive phases of granitoid plutonism, periods of felsic magma extrusion and hydrothermal alteration may explain the concentrations of Au and U in the Witwatersrand depository by providing a framework within which primary concentrations of metals might have taken place in the source area. The protracted emplacement of granite bodies until late in the depositional history of the basin, and the trend of increasingly younger detrital zircon grains upwards in the stratigraphic succession[1], indicate that the Witwatersrand source area was evolving continuously during basin formation. This might be the main reason why mineralization is almost entirely concentrated in the Central Rand group, whereas the underlying West Rand group remains largely barren. □

Received 12 December 1991; accepted 30 April 1992.

1. Robb, L. J., Davis, D. W. & Kamo, S. L. *J. Geol.* **98,** 311-328 (1990).
2. Barton, E. S. *et al. Econ. Geol.* **84,** 2012-2019 (1989).
3. Robb, L. J. & Meyer, F. M. *Econ. Geol.* **85,** 511-536 (1990).
4. Robb, L. J., Meyer, F. M., Drennan, G. R. & Ferraz, M. F. *S. Afr. J. Geol.* **93,** 5-40 (1990).
5. Armstrong, R. A., Compston, W., Retief, E. A., Williams, I. S. & Welke, H. J. *Precambr. Res.* **53,** 243-266 (1991).
6. Feather, C. E. & Koen, G. M. *Miner. Sci. Eng.* **7,** 189-224 (1975).
7. Handley, J. F. *Information Circ. Econ. Geol. Res. Unit,* Univ. Witwatersrand **227,** (1990).
8. Atomic Energy Corporation *Uranium in South Africa* (Pretoria, 1985).
9. Phillips, G. N. & Myers, R. E. *Econ. Geol.* **6,** 598-608 (1989).
10. Allsopp, H. L. & Welke, H. J. in *Mineral Deposits of Southern Africa* I (eds Anhaeusser, C. R. & Maske, S.) 495-496 (Geological Society of South Africa, Johannesburg, 1986).
11. Krogh, T. E. *Geochim. cosmochim. Acta* **37,** 485-494 (1973).
12. Krogh, T. E. *Geochim. cosmochim. Acta* **46,** 637-649 (1982).
13. Corfu, F. *Contrib. Miner. Petrol.* **98,** 312-325 (1988).
14. Davis, D. W. *Can. J. Earth Sci.* **19,** 2141-2149 (1982).
15. Drennan, G. R., Robb, L. J., Meyer, F. M., Armstrong, R. A. & de Bruiyn, H. *S. Afr. J. Geol.* **93,** 41-53 (1990).
16. Stacey, J. S. & Kramers, J. *Earth planet. Sci. Lett.* **26,** 207-221 (1975).
17. Key, R. M. & Wright, E. P. *J. geol. Soc. Lond.* **139,** 109-126 (1982).
18. Aldiss, D. N., Tombale, A. R., Mapeo, R. M. B. & Chiepe, M. *Bull. Geol. Surv. Dept Botswana* **33,** (1989).
19. Young, R. B. *The Blanket: A Study of the Auriferous Conglomerates of the Witwatersrand and the Associated Rocks* (Gurney & Jackson, London, 1917).

ACKNOWLEDGEMENTS. We thank J. Mortenson and J. Hodgson for reviews, and the Foundation for Research Development and the Anglo-American Corporation for financial and logistic support.

Causes of recent Himalayan uplift deduced from deposited patterns in the Ganges basin

Douglas W. Burbank

Department of Geological Sciences, University of Southern California, Los Angeles, California 90089-0740, USA

THE hypothesis[1] that late Cenozoic uplift of many of the world's mountain ranges was a response to climate change rather than to tectonic processes is based on the premise that enhanced erosion in an altered climate led to a reduction in both the total mass of a mountain range and its mean elevation. This reduction was coeval with increased regional relief and with passive isostatic uplift of the remaining summits. The hypothesis is difficult to evaluate because both climate and tectonic forces affect uplift in many active ranges. In the absence of sufficient denudational and uplift data from the mountains themselves, depositional patterns in adjacent basins may sometimes be used to distinguish between uplift arising from erosional or from tectonic processes. In foreland basins, uplift of the proximal basin and a reduction or absence of asymmetric subsidence are predicted responses to erosionally driven uplift[2]. Here I show that patterns of sediment accumulation and the position of major rivers in the Neogene Gangetic foreland basin seem to have changed markedly in Plio-Pleistocene times. These changes lend support to the hypothesis that the importance of erosional unloading has increased in the Himalayas during the past 4 Myr.

The record of considerable climate change leading to widespread glaciation during late Cenozoic times is unambiguous in many mountain ranges[3]. It is likely that repeated alpine glaciation led to enhanced rates of alpine erosion, but there is an absence of reliable data with which to calibrate changes either in the mean altitudes of uplifting ranges or in past sediment fluxes out of them. Here I examine the depositional patterns in basins that bound uplifting mountains and within which sediment eroded from nearby ranges was trapped. Development of two endmember models, one in which active tectonic shortening leads to mountain uplift and the other in which erosionally driven isostatic recovery leads to mountain uplift, can be used to predict contrasting depositional geometries. In the model, a mountain range adjacent to a foreland basin (Fig. 1) is underthrust by crust that behaves elastically, such that changes in the mass of the mountains cause flexural responses in the crust underlying the adjacent foreland basin[2,4-6]. In the foreland basin itself, there are two types of drainage systems: transverse systems draining perpendicular to the mountains and longitudinal systems flowing parallel to them[7]. The model predicts that the relative importance of transverse relative to longitudinal drainages can be interpreted in terms of erosion-driven against thrust-driven uplift.

If thrusting is the primary cause of mountain uplift, the resultant crustal thickening causes asymmetric subsidence within the adjacent foreland (Fig. 1*a*), such that considerably more subsidence and deposition occurs in the proximal parts of the foreland[4-6], and this subsidence inhibits the progradation of transverse fans across the basin. Transverse rivers are therefore restricted to proximal areas, and longitudinal or axial rivers flow along the medial part of the foreland near the fan toes (Fig. 1*c*). In cross-section, the basin will appear to be underfilled[5], because the rate of subsidence exceeds the rate of sediment supply to the transverse fans.

If enhanced erosion is the primary cause of uplift, isostatic recovery reduces the crustal root, and flexural uplift occurs across the foreland in response to the reduced mountain load (Fig. 1*b*). Enhanced erosion, however, leads to an increased flux of sediments into the basin, and this distributed sedimentary load, if preserved within the basin, both shifts the centre of loading away from the hinterland[5] and increases the width of the foreland basin. Along with possible uplift of the proximal foreland basin, subsidence across the foreland is less asymmetric because of the distributed sedimentary load. Reduced subsidence in the proximal foreland and enhanced flux of sediments into the basin cause transverse fans to expand and longitudinal rivers to be displaced toward the distal basin (Fig. 1*d*). These models suggest that, despite a paucity of uplift and erosion data from a given mountain range, we can use the presence or absence

of asymmetric subsidence, a tabular rather than wedge-shaped geometry of sedimentary strata, and the relative importance of longitudinal or transverse rivers within an adjacent foreland basin, to differentiate between tectonically driven and erosionally driven uplift.

Depositional geometries within the Himalayan foreland basin can be evaluated in the context of these models to suggest which process is primarily responsible for late Cenozoic uplift of the Himalaya. The Indo-Gangetic foreland basin is developed in front of the transpressional ranges of western Pakistan and the collisional ranges of the Himalaya and Karakoram, and its strata onlap the western and northern margins of the Indian subcontinent. The huge volumes of sediment stored in the Bengal and Indus fans[8,9] indicate that, throughout the past 20 Myr, the foreland has been nearly continuously filled to overflowing, such that all available sediment accommodation space was occupied. Assuming a relatively homogeneous rheology for the Precambrian crust of the Indian sub-continent[10], the flexural wavelengths (~300 km) of the Indus and the Gangetic forelands should be similar. There is, however, a strong contrast in the modern drainage geometries observable in these two basins (Fig. 2*a*). Once it enters the foreland in northern Pakistan, the Indus River is rarely more than 100 km from the mountain front, and in many cases, such as with respect to the Sulaiman and Kirthar ranges, it flows longitudinally very close to the range front despite the presence of a broad, largely undeformed foreland in the medial and distal portions of the basin. These geometries seem to result from rapid asymmetrical subsidence and/or a relatively low sediment flux from the transverse fans. Except where the Indus drainage flows within the Hindu Kush and Himalaya, most of its bounding mountain ranges are relatively low in elevation (<2 km), are located within a semi-arid to arid climate regime, and have experienced little or no glacial erosion. These factors[11] should combine to provide a smaller transverse sediment flux into the middle and lower Indus River than in its course within the Himalaya.

A strongly contrasting scenario is seen in the Ganges foreland basin (Fig. 2*a*). Except in the headward part of the drainages, the Yamuna and Ganges rivers form a longitudinal system flowing parallel to, but 200–300 km in front of, the mountain front. For much of their courses, these rivers are in the most distal part of the foreland basin, often along the feather edge. Although the foreland strata thicken to more than 6 km adjacent to the mountain front, the foreland basin strata beneath the modern Ganges and Yamuna rivers are typically <1 km in thickness. Large, low-gradient transverse fans dominate the proximal and medial parts of the Ganges foreland basin. The progradation of these transverse fans has pushed the Ganges River into its present, very distal position. The cross-sectional asymmetry of the Neogene Ganges foreland fill[12] indicates that thrust loading has been the primary long-term (pre-Pliocene) control on basin subsidence (Fig. 2). The present drainage pattern and the cross-sectional geometry of the Plio-Holocene basin fill (Upper Siwalik: Fig. 2*b* and *c*), however, support a model in which erosional unloading has propelled late Cenozoic uplift of both the range and the proximal foreland basin, and in which increased sediment fluxes into the foreland have led to extensive progradation of more tabular transverse fans, as opposed to the prismatic geometries that prevail during times of asymmetries subsidence (Lower and Middle Siwalik, Fig. 2*b* and *c*).

The anomalous nature of the modern situation can be discerned through comparison with the geometries that prevailed during middle and late Miocene times, when the ancestral Indus River in northeastern Pakistan flowed east-southeast into the Ganges drainage[7,13] and was part of a longitudinal river system that flowed along virtually the entire front of the Himalayan range. Although erosion or overthrusting of Miocene rocks precludes description of the drainage patterns in the most proximal part of that basin, preserved fluvial strata clearly indicate that the ancestral Indus–Ganges system flowed in the medial part of the basin and was often located far (>100 km) from the distal edge of the basin[7,14]. Unlike the modern Ganges River, this ancestral river typically flowed along the surface of >2 km of previously accumulated strata in a foreland basin characterized by subsidence that was strongly asymmetric toward the hinterland. Synchronous intervals of accelerated subsidence[15–17] suggest that thrust loading in the hinterland, probably including major basement-involved thrusts, were the primary controls on the subsidence and the basin-filling history during Miocene times.

Additional information comes from tectonic, stratigraphic and geomorphological data. First, because the rate of Indo-Asian convergence has not slowed significantly since Miocene times, any diminution in the rate of thrust loading within the Himalaya must be attributed to changes in the regional partitioning of

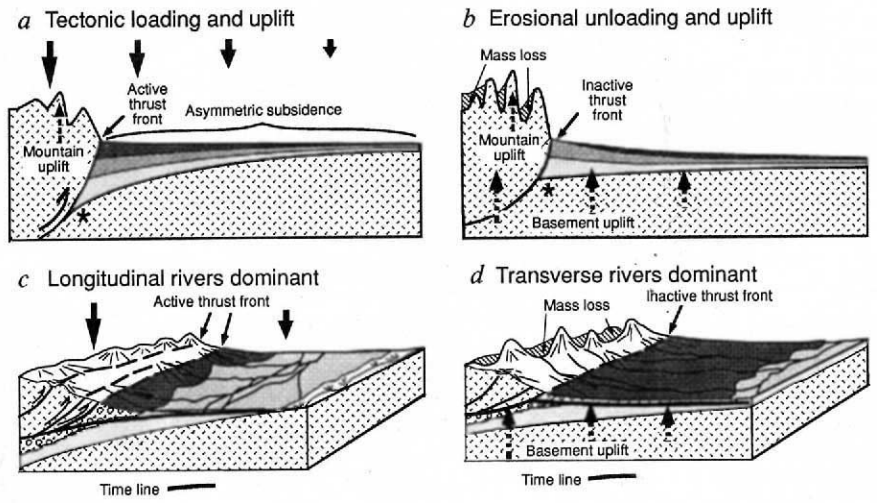

FIG. 1 Schematic contrasts in subsidence and depositional patterns in foreland basins adjacent to mountains undergoing either tectonic loading or erosional unloading. Both scenarios cause uplift of individual summits, but during erosional unloading the mean surface elevation dereases. *a*, Tectonic loading due to crustal compression and thickening drives both uplift of the mountain summits (dashed arrow) and asymmetric subsidence (heavy arrows) in the foreland basin above an elastically loaded crust, such that wedge-shaped depositional units thicken toward the thrust front (* marks reference point at top of basement). *b*, Erosional unloading causes isostatic uplift of remaining peaks as the total mass of the mountains is reduced. Topography of the tectonically generated mountains (from *a*) is superimposed (hachured area) to show the net loss of mass despite summit uplift. Because of the elastic crustal response, the proximal foreland basin is also uplifted (heavy dashed arrows indicate basement uplift) and may be eroded. In cross-section, new sedimentary deposits are tabular, rather than wedge-shaped. *c*, Depositional patterns during active thrust loading are characterized by short transverse rivers and dominant longitudinal rivers flowing in the distal and medial parts of the foreland, often above several kilometres of previously deposited fluvial strata. Stratal time line illustrates asymmetric subsidence. *d*, During the erosional phase, there is a net mass loss from the mountains (hachured area represents eroded topography of Fig. 1*c*), widespread basement uplift occurs, transverse rivers prograde across the foreland, and the longitudinal river is restricted to a distal position above thin to negligible previously deposited foreland strata.

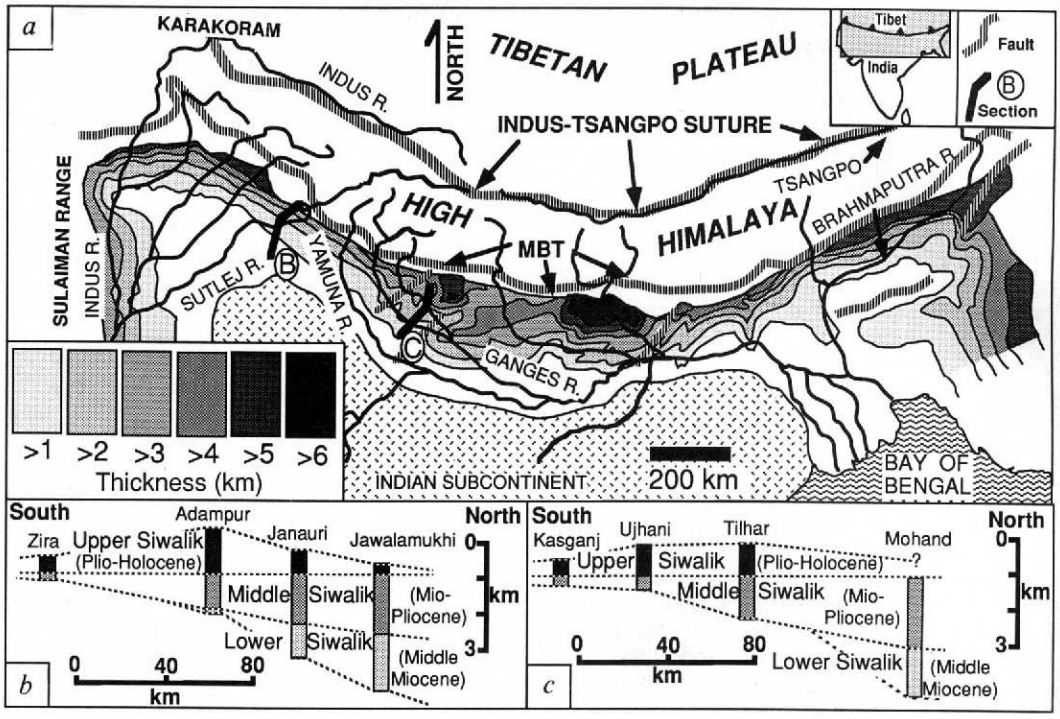

FIG. 2 *a*, Major drainage patterns in the Himalayan system and isopach map of foreland strata (in kilometres of preserved thickness). An asymmetric wedge of sedimentary rocks thickens toward the mountain front along the entire range. After entering the foreland south of the main boundary thrust (MBT), the Indus flows as a longitudinal river parallel and close to the front of the Sulaiman and Kirthar Ranges. In contrast, after flowing as transverse rivers across the thick, pre-Pleistocene deposits of the Ganges foreland, the Yamuna and Ganges become longitudinal rivers restricted to the extreme distal margin of the depositional basin, a position consistent with transverse-fan progradation in response to erosional unloading in the main Himalayan Range. Major faults are shown by vertically hachured lines. Locations of cross-sections (*b*, *c*) are shown by heavy solid lines. *b*, *c*, Schematic transverse cross-sections of the Ganges foreland based on drill-hole data[29] showing stratal thickening toward the mountains during Middle and Lower Siwalik deposition, and stratal thickening away from the mountains and more tabular depositional geometries during Upper Siwalik deposition from the Pliocene until present. Location of sections is shown by labelled lines in *a*.

shortening. Accelerated Plio-Pleistocene deformation in the Tien Shan and northeastern Tibet[18–21] may be accommodating some of the convergence that was previously absorbed by the Himalaya. Second, although there is clear evidence of Pleio-Pleistocene shortening in the Himalaya[12,22,23], rates of denudation nearly equivalent to the rate of hanging-wall uplift[24] have often reduced the expected thrust loads within rapidly deforming areas. Third, modern levelling studies in the Nepal Himalaya[25] show that, despite ongoing uplift in the High Himalaya and the proximal foreland, the mean rate of erosional lowering at present exceeds the rate of interseismic uplift. Finally, during the Pliocene epoch at a time of accelerating uplift in the outer ranges of the Himalaya[22] and rapidly changing climate[26], the longitudinal drainage system (the ancestral Indus River) in the northwestern Himalaya was displaced by a transverse system (the ancestral Jhelum River)[13,27]. This change was partially in response to relative uplift of the proximal foreland and an outward displacement of the depocenter[16,28] and was accompanied by a grain-size coarsening and possibly an enhanced sediment flux out of the Himalaya.

The timing of the transition to a Gangetic foreland dominated by transverse rivers is poorly constrained. In northern Pakistan, it is younger than ~4 Myr (refs 13, 22, 27, 28), but the transition can only be defined as occuring during Upper Siwalik (Plio-Pleistocene) deposition in India[14,29]. Nevertheless, these ages post-date by ≥4 Myr the estimated time when the Tibetan Plateau achieved nearly its present height ~8 Myr (ref. 30) and the apparently related initiation of the Indian monsoon[31]. Although considerable time-lag could be invoked to correlate the river-pattern transition with these tectonically driven events, it seems more closely linked in time to the initiation of widespread Northern Hemispheric continental and alpine glaciation during late Pliocene times[3,26,32].

This analysis shows that simple models predict very different responses for the depositional systems in foreland basins adjacent to ranges in which summits are uplifting because of thrust thickening and ones in which uplift is in response to erosion and isostatic recovery. Although the relative importance of erosionally driven and tectonically driven uplift today or in the past is not precisely known, the data from the modern Indus and the Miocene Indo-Gangetic forelands suggest that thrust loading in the hinterland generated asymmetric subsidence, inhibited progradation of transverse fans and permitted longitudinal river systems to flow in medial or even proximal parts of the foreland basin. Despite evidence of active thrusting and local crustal thickening in parts of the Himalaya today, the modern Gangetic foreland is dominated by transverse drainages. Large Plio-Pleistocene sediment fluxes combined with both broadly distributed, less asymmetric subsidence and uplift of the proximal foreland have led to extensive progradation of transverse drainage systems that displaced the Ganges River to the feather edge of the present foreland basin: a position that is consistent with erosion-driven uplift in the adjacent Himalaya, but would be highly anomalous if thrust-driven crustal thickening were the primary cause of uplift in those same mountains. Improved calibration of changes in Neogene to Quaternary sediment fluxes into the Indo-Gangetic foreland and in surface elevations within the Himalaya are needed to evaluate this hypothesis more completely. □

Received 15 January; accepted 8 May 1992.

1. Molnar, P. & England, P. *Nature* **346,** 29–34 (1990).
2. Heller, P. L., Angevine, C. L., Winslow, N. S. & Paola, C. *Geology* **16,** 501–504 (1988).
3. Sibrava, V., Bowen, D. Q. & Richmond, G. M. *Quaternary Glaciations in the Northern Hemisphere* (Quat. Sci. Rev. 5) (1986).
4. Flemings, P. B. & Jordan, T. E. *J. geophys. Res.* **94,** 3851–3866 (1989).
5. Flemings, P. B. & Jordan, T. E. *Geology* **18,** 430–434 (1990).
6. Angevine, C. L., Heller, P. L. & Paola, C. *Quantitative Sedimentary Basin Modelling* (American Association of Petroleum Geologists, Tulsa, 1990).
7. Burbank, D. W. & Beck, R. A. *Geol. Rund.* **80** (1991).
8. Naini, B. P. thesis, Columbia Univ. (1980).
9. Curray, J. R. *Geology* **19,** 1097–1100 (1991).
10. Molnar, P. *A. Rev. Earth planet. Sci.* **12,** 489–518 (1984).
11. Ahnert, F. *Am. J. Sci.* **268,** (1970).
12. Raiverman, V., Kunte, S. V. & Mukherjea, A. *Petrol. Asia J.* 67–92 (1983).
13. Raynolds, R. G. H. thesis, Dartmouth College (1980).
14. Tandon, S. K. & Rangaraj, S. in *Structural Geology of the Himalaya* (ed. Saklani, P. S.) (Today and Tomorrow's Printers and Publishers, Delhi, 1979).
15. Burbank, D. W. & Beck, R. A. *Geol. Bull. Univ. Peshawar* **22,** 11–24 (1989).
16. Burbank, D. W., Beck, R. A. & Talling, P. J. *Geol. Soc. Am. Abst. Prog.* **23,** 241 (1991).
17. Johnson, N. M., Stix, J., Tauxe, L., Cerveny, P. F. & Tahirkheli, R. A. K. *J. Geol.* **93,** 27–40 (1985).

18. Molnar, P., Burchfiel, B. C., K'uangyi, L. & Zhao, Z. *Geology* **15,** 249–253 (1987).
19. Molnar, P. *et al. Geol. Soc. Am. Abstr. Prog.* **23,** 373 (1991).
20. Burchfiel, B. C. *et al. Tectonics* **10,** 1091–1110 (1991).
21. Zhang, P. *et al. Tectonics* **10,** 1111–1129 (1991).
22. Burbank, D. W. & Raynolds, R. G. H. in *New Perspectives in Basin Analysis* (ed. Kleinspehn, K. L. & Paola, C.) (Springer, New York, 1988).
23. Karunakaran, C. & Rao, A. R. *Geol. Sur. India Misc. Publ.* **41,** 1–66 (1979).
24. Burbank, D. W. & Beck, R. A. *Geology* **19,** 1169–1172 (1991).
25. Adhikari, K. *et al. Eos Trans.* **72,** 496 (1991).
26. Liu, T. *Aspects of Loess Research* (China Ocean, Beijing, 1987).
27. Burbank, D. W., Beck, R. A., Raynolds, R. G. H., Hobbs, R., Takirkheli, R. A. K. *Geology* **16,** 1143–1146 (1988).
28. Raynolds, R. G. H. & Johnson, G. D. in *The Chronology of the Geologic Record* (ed. Snelling, N. J.) (Geological Society of London, 1985).
29. Acharyya, S. K. & Ray, K. K. *AAPG Bulletin* **66,** 57–70 (1982).
30. Harrison, T. M., Copeland, P., Kidd, W. S. F. & Yin, A. *Science* **255,** 1663–1670 (1992).
31. Prell, W. L. & Kutzbach, J. E. *Eos* **72,** 257–258 (1991).
32. Shackleton, N.J. *et al. Nature* **307,** 620–623 (1984).

ACKNOWLEDGEMENTS. I thank R. Beck and T. Muller for assistance in the field, and members of the University of Peshawar, particularly R. A. K. Tahirkeli and J. Khan, for support. The sedimentary isopach base map was provided by Bob Raynolds. This research was partially funded by the NSF and National Geographic Research.

A vascular conducting strand in the early land plant *Cooksonia*

D. Edwards, K. L. Davies & L. Axe

Department of Geology, University of Wales College of Cardiff, PO Box 914, Cardiff CF1 3YE, UK

THE late Silurian–early Devonian genus *Cooksonia*, characterized by smooth isotomously branching axes and solitary, terminal sporangia[1], has long been regarded as the archetypal vascular plant because of its age and simplicity of organization. The discovery of stomata, sterome[2] and thick-walled spores[1,3] in *Cooksonia pertoni* and *C. hemisphaerica* confirmed its land-plant status, but tracheids have never been demonstrated in attached axes[4]. Here we report on tubes with differentially thickened walls typical of tracheary elements found in the central region of axes of Lower Devonian unequivocal *C. pertoni*, vindicating Lang's belief that *Cooksonia* was a vascular plant[1].

The specimens come from the same stream section through Lower Old Red Sandstone fluviatile sediments on Brown Clee Hill, Shropshire, that have yielded the well preseved *C. pertoni*[2,3]. Spore assemblages indicate a Gedinnian age (middle *micrornatus-newportensis* miospore assemblage subzone)[5]. The fossils are coalified, partially compressed, showing remarkable preservation of axial and sporangial cells, and occasionally *in situ* spores. They were recovered from the residue left after dissolving the grey silty matrix with hydrofluoric acid. After secure identification involving scanning electron microscopy, two specimens were prepared for sectioning. Axes were separated from sporangia, treated with fuming nitric acid for 30 min, washed thoroughly and dehydrated in 100% acetone. After passing through increasing ratios (1 : 3, 1 : 1, 3 : 1) of low-viscosity Spurr resin to acetone (modified from ref. 6), they were embedded in Spurr resin[7] and polymerized for 24 h at 70 °C. Specimens were sectioned using an LKB Ultratome 8801A with glass knives and 60–90 nm-thick sections (UF597 series) were collected on collodion-coated copper grids and stained with potassium permanganate, uranyl acetate and lead citrate (modified from ref. 6) before transmission electron microscopy using a JEOL 100S at an accelerating voltage of 80kV. For light microscopy, sections of 1 μm thickness (UF1877 series) were stained with 0.25% (w/v) toluidine blue in 0.25% (w/v) sodium tetraborate solution, air-dried, and mounted in Elvacite.

Figure 1*a* shows a stalked sporangium with a shape typical of *C. pertoni*[3]. The well-preserved *in situ* spores belong to the dispersed taxon *Streelispora newportensis* (Fig. 1*d*) and identify the specimen as *C. pertoni* ssp. *apiculispora*[3]. The sporangium has a well defined rim with numerous papillate cells (Fig. 1*c*), not previously recorded. The subtending axis, although short and apparently shrivelled, shows at least eight stomata (Fig. 1*b*), but remaining epidermal cells are indistinct. Its fractured end reveals fragmentary cell walls and abundant isolated pyrite octahedra that disrupt and distort cellular organization. Towards the centre of the axis are fragments of 2–3 cells with thickenings similar to those in the xylem of tracheophytes (Fig. 2*b*). Where intact, the external wall may be smooth or corrugated, depressions marking the positions between secondary thickenings. The latter appear annular with some interconnections (Fig. 2*b*). A fractured portion of the same tracheid shows a cast of the lumen, indentations marking the positions of the secondary wall, and also the inner surface of the tracheid wall with thickenings (Fig. 2*a*). At high magnifications, the coalified walls appear granular, but lack indications of further pitting as, for example, characterizes *Gosslingia*[8]. Owing to their incomplete nature, it cannot be decided whether these elements with differentially thickened walls are tubes or tracheids, but the latter seem most likely. Dimensions are given in Table 1. Longitudinal sections through fragments of tracheids have been observed by transmission electron microscopy (Fig. 3*a–b*) and by light microscopy (Fig. 3*c–f*). The best example of the former (Fig. 3*b*)

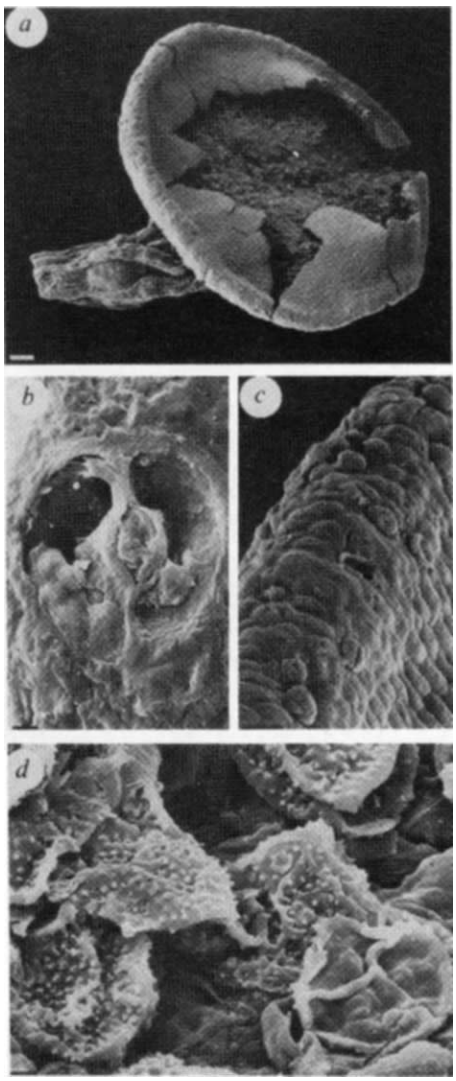

FIG. 1 Scanning electron microscopy (SEM; Cambridge microscope S360) of *Cooksonia pertoni* ssp. *apiculispora*. Gedinnian Shropshire (DE41). *a*, Complete specimen with short stalk (scale bar, 100 μm); *b*, stoma (scale bar, 5 μm); *c*, sporangial rim with papillate cells (scale bar, 30 μm); *d*, *in situ* spores from the dispersed taxon *Streelispora newportensis*, although this specimen lacks the characteristic proximal folding (scale bar, 5 μm).